BNL-111872-2016-IR

eRHIC/51
February 2016

An electron storage ring proposal for the Ring-Ring eRHIC project

S. Tepikian, M. Blaskiewicz, C. Montag, S. Peggs

Collider-Accelerator Department
Brookhaven National Laboratory
Upton, NY 11973

U.S. Department of Energy
Office of Science, Office of Nuclear Physics

Notice: This document has been authorized by employees of Brookhaven Science Associates, LLC under Contract No. DE-SC0012704 with the U.S. Department of Energy. The United States Government retains a non-exclusive, paid-up, irrevocable, world-wide license to publish or reproduce the published form of this document, or allow others to do so, for United States Government purposes.

An Electron Storage Ring Proposal for the Ring-Ring eRHIC Project

S. Tepikian, M. Blaskiewicz, C. Montag, S. Peggs

A design of the Ring-Ring eRHIC electron storage ring is proposed. This design will cover three energy configurations denoted as *Low*, *Middle* and *High*. The requirements for this ring are defined in the baseline Table 1. This ring must fit in the existing RHIC tunnel and the circumference has to match that of RHIC.

	Low	**Middle**	**High**
Energy [GeV]	5	20	20
Magnetic Rigidity: Bρ [T-m]	16.6782	66.7128	66.7128
Bunch Population [10^{11}]	2.08	1.14	1.14
Number of Bunches	360	360	360
Beam Current [A]	0.925	0.508	0.508
Energy loss per turn: U_0 [MeV]	0.18	47.1	47.1
Arc SR Power: P_{arc} [MW]	0.2	23.9	23.9
Emittance: ε_H, ε_V [nm]	106.0, 19.0	62.2, 11.2	53.0, 9.5
IP betas: β_H, β_V [m]	0.86, 0.60	0.61, 0.42	0.38, 0.27

Table 1: The baseline design goals for the electron storage ring [1].

The ring is designed to be modular consisting of: (1) arc cells, (2) dispersion suppressors, (3) three straight sections without dispersion, (4) a straight section with dispersion which includes a Robinson Wiggler [2] to control the emittance in the low energy configuration and (5) two low-β IRs that can operate in both colliding and non-colliding mode. The following sections discuss these different beam line sections.

Cell Choice

There are many cell configurations available that are used in electron storage rings [2][3]. Their goal is to achieve a low emittance. But, this often leads to a low packing factor for the dipoles. A basic rule of thumb is, the lower the packing factor, the lower the emittance that can be achieved. Since, a high packing factor leads to longer dipoles, thus, lower dipole field and in turn lower electron radiation – for high energy operation – this reduces operational cost. Furthermore, moderate emittances are required for the baseline. Three cell types given below are considered:

1. FODO cell. A standard cell structure shown in Fig 1.
2. TBA cell. Triple Bend Achromat shown in Fig 2.
3. TAL cell. Triplet Achromat Lattice shown in Fig 3.

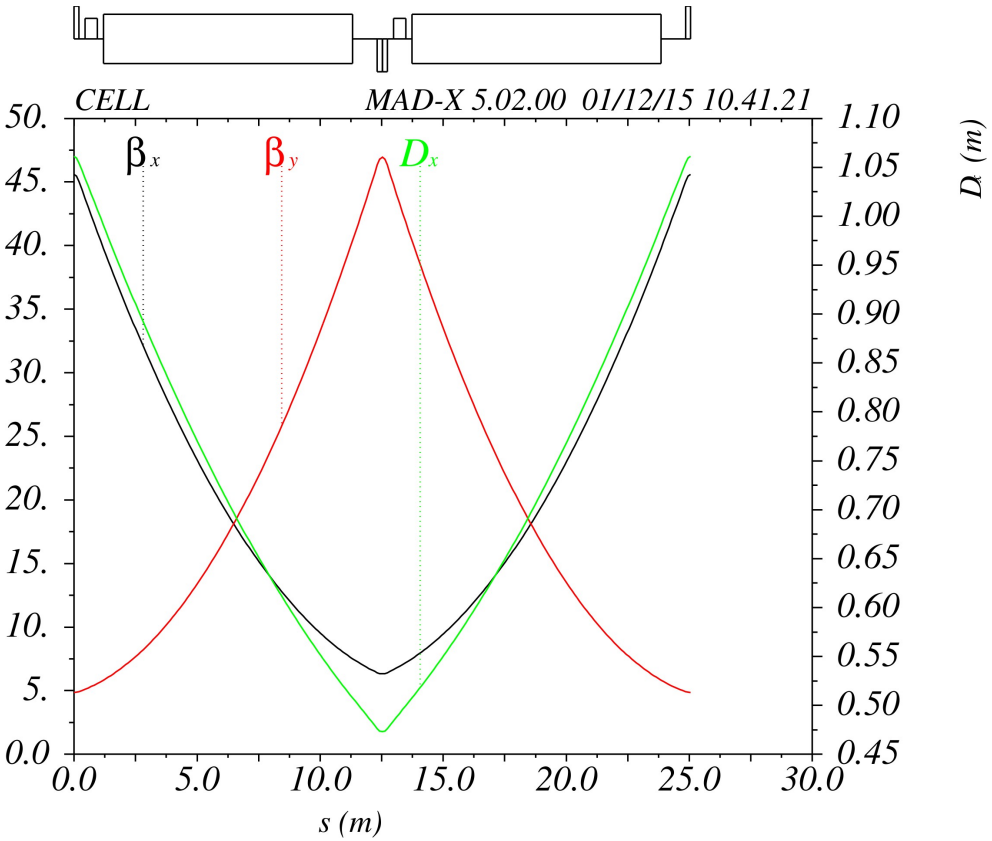

Figure 1: A standard FODO cell.

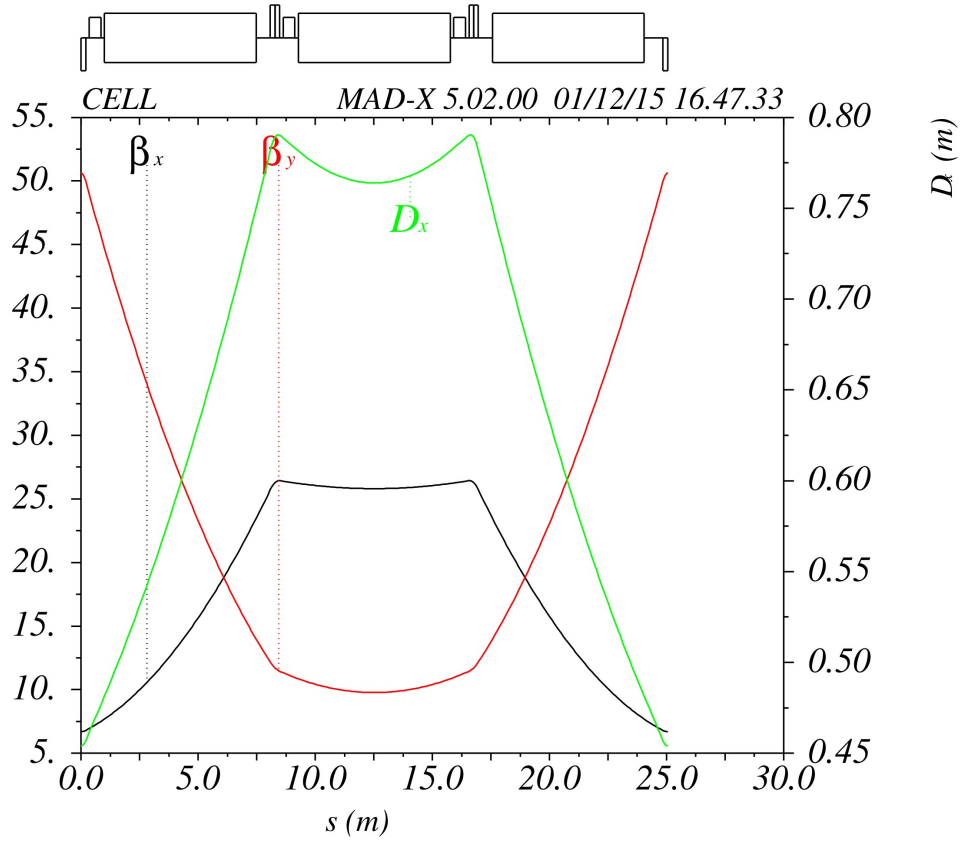

Figure 2: Triple Bend Achromat (TBA) cell.

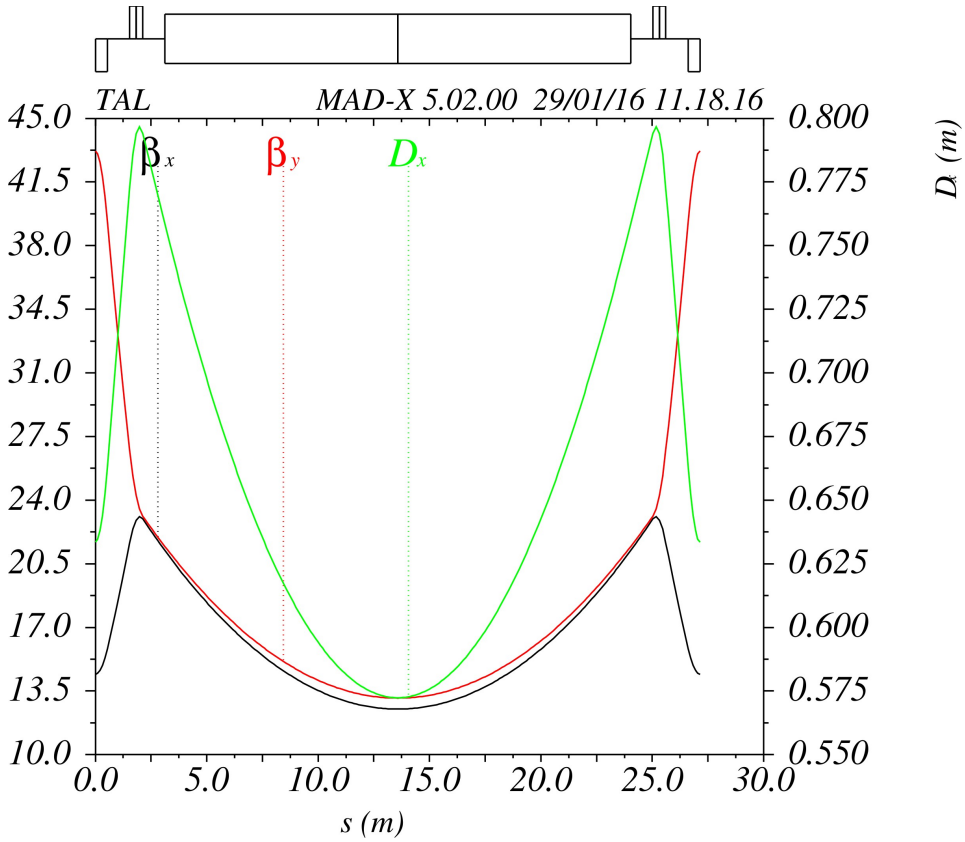

Figure 3: Triplet Achromat Lattice (TAL) cell.

The TAL cell loses out for two reasons. The quadrupole strengths are higher than the other cells require, thus longer quadrupoles are needed, reducing the packing factor. Furthermore, the chromatic correction becomes more difficult with this cell.

Next, the TBA cell shows a lot of promise and a full ring was designed with this cell. In order to reduce the packing factor, the drift spaces between the magnets were reduced. This adds a constraint if we wish to use existing quadrupoles such as those available from PEP II [4]. Furthermore, the lower dispersion leads to stronger sextupoles for chromatic correction and larger higher-order chromatic effects.

Finally, the FODO cell gives the highest packing factor and has the space to use the longer PEP II quadrupoles. The requested baseline emittances are achievable with this cell. The higher order chromatic effects are reasonable with two families of sextupoles. Final results are shown in Table 5.

Tables 2-4 shows the horizontal cell phase advance at various energies and cell lengths to get an emittance of 53 nm. The TAL cell has significantly lower dipole bending radius, ρ, which will lead to high power requirements, which is more than the baseline parameters. The TBA cell has more moderate dipole bending radius, but may still have some difficulty in reaching the baseline power requirements. The FODO cell which has dipoles with the longest bending radius will be able to meet the baseline power requirements and achieve the emittance requirements as well. For these reasons, the FODO cell has been chosen. The 2.4 m space – in the FODO cell – between the dipoles gives enough room to use the existing PEP II quadrupoles.

FODO Cell

					Horizontal Phase Advance at 53 nm [°]			
N_{cells}	L_{cell} [m]	L_D [m]	ρ [m]	PF [%]	5 GeV	10 GeV	15 GeV	20 GeV
16	27.8166	11.5083	307.7095	72.4011	41.6609	66.7309	89.2446	113.0798
17	26.1803	10.6902	306.2509	72.0579	39.0228	62.3768	83.0294	103.6440
18	24.7259	9.9629	304.4450	71.6330	36.7232	58.6099	77.7638	96.2944
19	23.4245	9.3123	302.3468	71.1393	34.7012	55.3159	73.2226	90.2180
20	22.2533	8.7266	300.0000	70.5871	32.9096	52.4095	69.2544	85.0392
21	21.1936	8.1968	297.4402	69.9848	31.3115	49.8256	65.7512	80.5409
22	20.2303	7.7151	294.6964	69.3392	29.8774	47.5130	62.6328	76.5813

Table 2: Horizontal FODO cell phase advance in degrees for different cell lengths at various energies in an arc with a length of 445.06585 m and total bend angle of 60° including dispersion suppressors at the ends.

TBA Cell

					Horizontal Phase Advance at 53 nm [°]			
N_{cells}	L_{cell} [m]	L_D [m]	ρ [m]	PF [%]	5 GeV	10 GeV	15 GeV	20 GeV
16	27.8166	7.4055	297.0143	69.8846	41.9471	66.9532	88.9205	110.7265
17	26.1803	6.8601	294.7917	69.3617	39.3400	62.7070	83.0356	102.5534
18	24.7259	6.3753	292.2219	68.7570	37.0671	59.0228	77.9963	95.8703
19	23.4245	5.9415	289.3597	68.0836	35.0687	55.7951	73.6200	90.2112
20	22.2533	5.5511	286.2490	67.3517	33.2984	52.9438	69.7781	85.3198
21	21.1936	5.1979	282.9252	66.5696	31.7200	50.4071	66.3758	81.0324
22	20.2303	4.8768	279.4175	65.7443	30.3046	48.1364	63.3406	77.2353

Table 3: Horizontal TBA cell phase advance in degrees for different cell lengths at various energies in an arc with a length of 445.06585 m and total bend angle of 60° including dispersion suppressors at the ends.

TAL Cell

					Horizontal Phase Advance at 53 nm [°]			
N_{cells}	L_{cell} [m]	L_D [m]	ρ [m]	PF [%]	5 GeV	10 GeV	15 GeV	20 GeV
16	27.8166	21.5776	288.4715	67.8746	41.6390	65.4730	85.1787	102.7059
17	26.1803	19.9413	285.6387	67.2081	39.1500	61.5768	80.0981	96.4632
18	24.7259	18.4869	282.4587	66.4598	36.9780	58.1780	75.6810	91.0936
19	23.4245	17.1855	278.9863	65.6428	35.0673	55.1882	71.8030	86.4085
20	22.2533	16.0143	275.2654	64.7673	33.3749	52.5394	68.3711	82.2777
21	21.1936	14.9546	271.3314	63.8417	31.8665	50.1782	65.3135	78.6057
22	20.2303	13.9913	267.2135	62.8728	30.5150	48.0618	62.5736	75.3201

Table 4: Horizontal TAL cell phase advance in degrees for different cell lengths at various energies in an arc with a length of 445.06585 m and total bend angle of 60° including dispersion suppressors at the ends.

Dispersion Suppressor

The dispersion suppressor, denoted as DS, consists of three cells at both ends of each ARC. Thus, the ARC contains all the bending in the ring. A general DS is shown in Fig. 4.

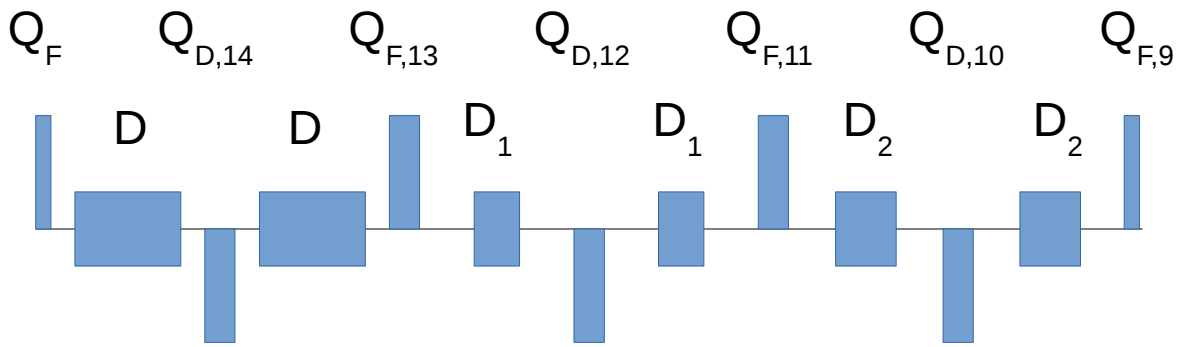

Figure 4: Basic dispersion suppressor made of three FODO cells. The lengths of the dipoles D_1 and D_2 are adjusted till the dispersion and its derivative are zero after $Q_{F,9}$. Note, the dipole lengths depends on the horizontal phase advance of the FODO cell. The quadrupoles $Q_{D,14}$ through $Q_{F,9}$ are adjustable for the cases when the horizontal phase advance is different.

The DS depends on the horizontal phase advance of the cell. From Fig. 4, the regular cell dipole is denoted with, D, and the additional dipoles: D_1 and D_2 are for the dispersion suppression. The bending angle of the dipoles D_1 and D_2 are determined from [5] as:

$$\lambda = \frac{1}{4\sin^2(\mu/2)} \qquad \theta_1 = (1-\lambda)\theta \qquad \theta_2 = \lambda\theta$$

where μ is the horizontal phase advance of the cell, θ_1 is the bending angle of dipole D_1, θ_2 is the bending angle of dipole D_2 and θ is the bending angle of dipole D. This formula also works for the TBA and TAL cells as well. For cells whose phase advance differs from μ, six quadrupoles are adjusted to keep the dispersion suppressed and have the same cell Twiss parameters (six constraints) at the end of the DS. Note, when the quadrupoles are changed their corresponding Twiss parameters will no longer be cell-like within the DS. Some of the beta functions can become quite large, so the choice of μ is important. For this ring after a few tries, we settled on μ=60° horizontal phase advance. Thus, D_1 becomes empty and D_2=D. Figs. 5-7 show the final results for the three energy configurations.

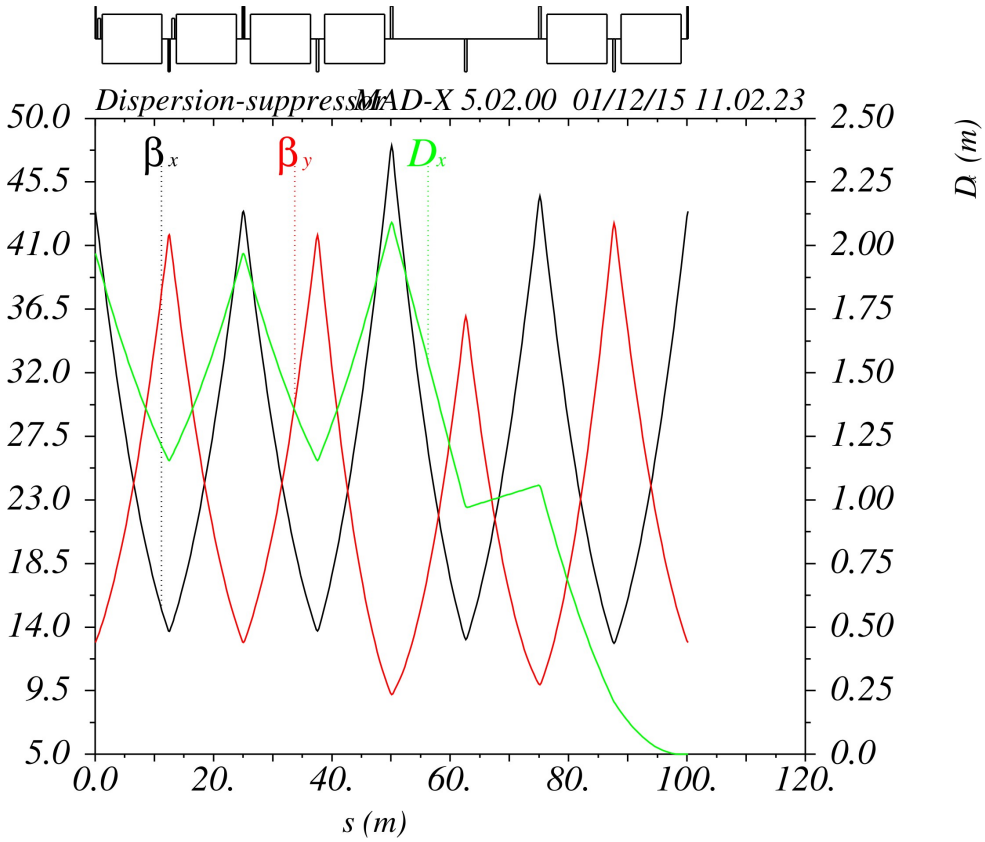

Figure 5: Dispersion suppressor for the low energy configuration. Cell horizontal phase advance is about 61.76°.

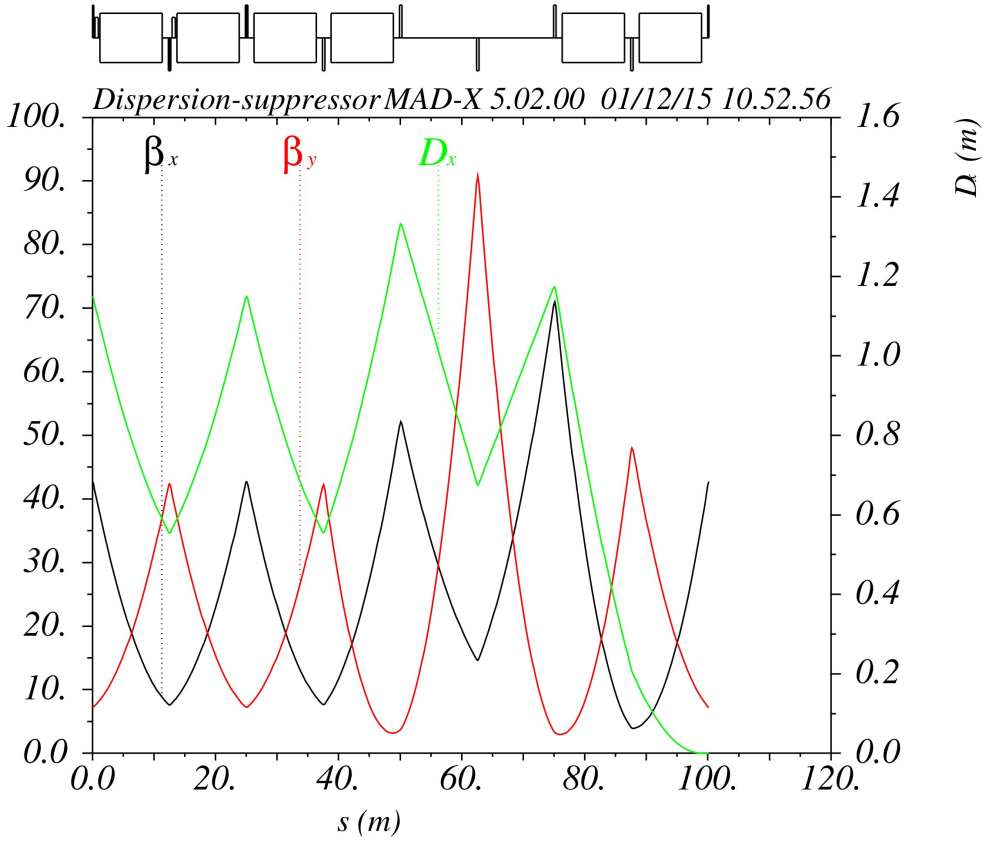

Figure 6: Dispersion suppressor for the middle energy configuration. Cell horizontal phase advance is about 88.06°.

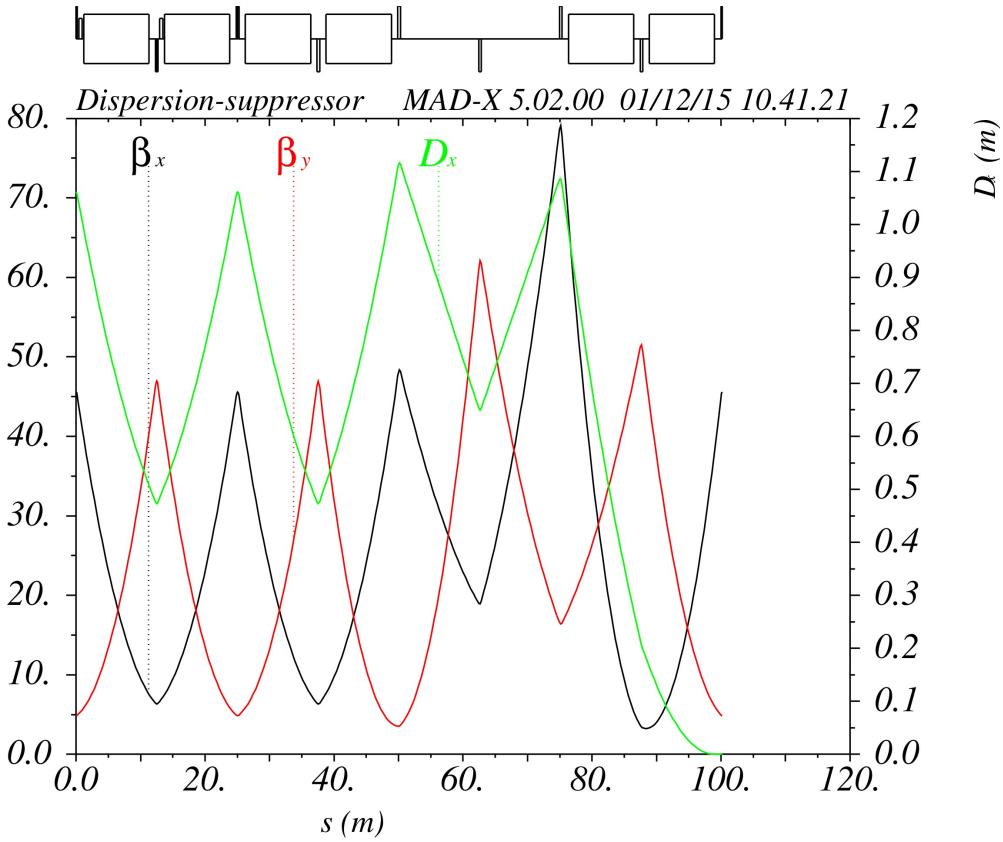

Figure 7: Dispersion suppressor for the high energy configuration. Cell horizontal phase advance is about 95.07°.

ARC

The arc consists of 12 FODO cells plus two DSs (3 cells per DS) at each end[1]. The ring consists of 6 ARCs with straight sections between them. The total bending angle of the ARC must be 60°=360°/6. The total circumference of the ring is set to 3833.845181 m to match the RHIC ring. Finally, the length of the ARC, 450.857709 m, is determined such that the IP points of this ring match the IP points of RHIC. Thus, the lengths of the straight sections between the ARCs is determined to be 188.116488 m. Fig. 8 shows the ARC for the high energy configuration.

There are 18=3+12+3 cells needed per arc. Thus, each cell has a length of 25.047651 m. Since, the space allocated for the quadrupoles, BPMs, correctors, sextupoles, etc, is 2.4 m between the dipoles, the dipole length is 10.123825 m. Taking into account the DSs, there are 32 dipoles per ARC. This leads to a dipole bending radius of ρ=309.361304 m.

1 There is one straight section that has dispersion present. In this case the DSs about this straight section are replaced by three cells where the last cell has no dipoles.

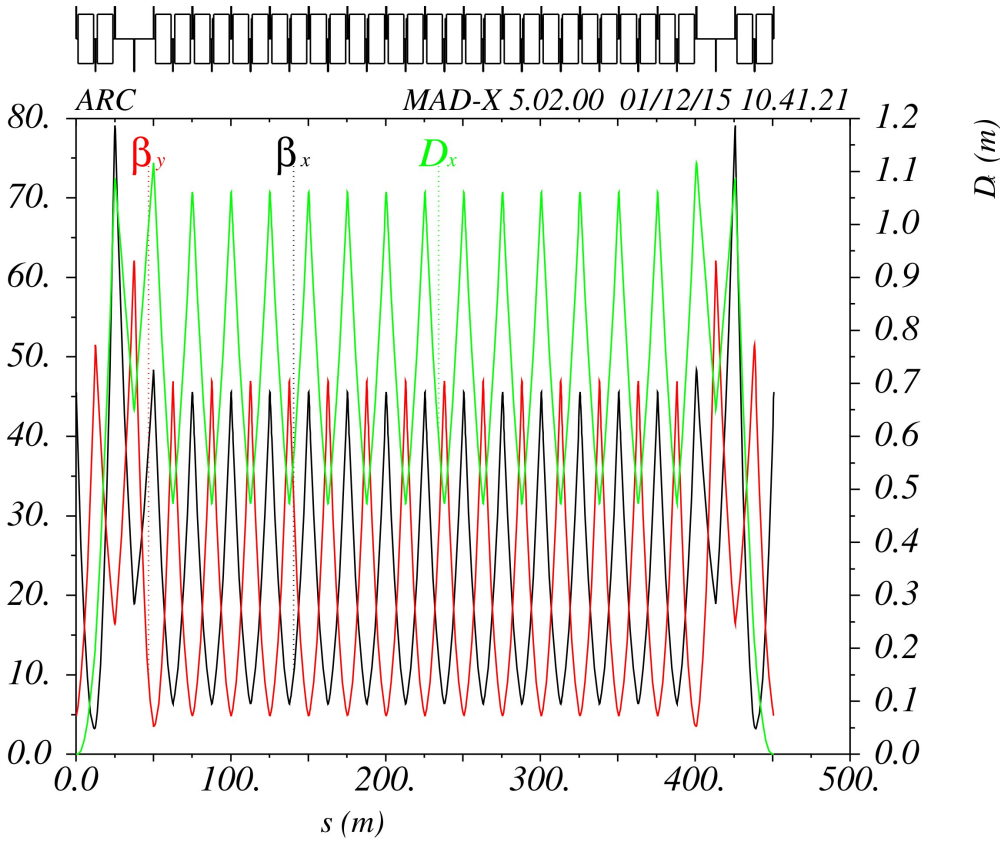

Figure 8: One of six ARCs in the ring for the high energy configuration.

Colliding IP (Dispersion Free)

Two of the straights will have optics for colliding the electron beam with beam in the RHIC ring. The optics for these sections are symmetric. Each energy configuration has different β^* at the collision point (IP), see Table 1. The high energy configuration has the smallest β^*=(0.38 m, 0.27 m) at the IP and largest β_{max}=604 m. These sections can also be set to non-colliding mode with a larger β^* at the IP and a smaller β_{max}. This section includes a large empty drift space of 35 m long for spin rotators and other devices as needed. Fig. 9-10 shows the optics for this section in both high energy colliding mode and non-colliding mode respectively.

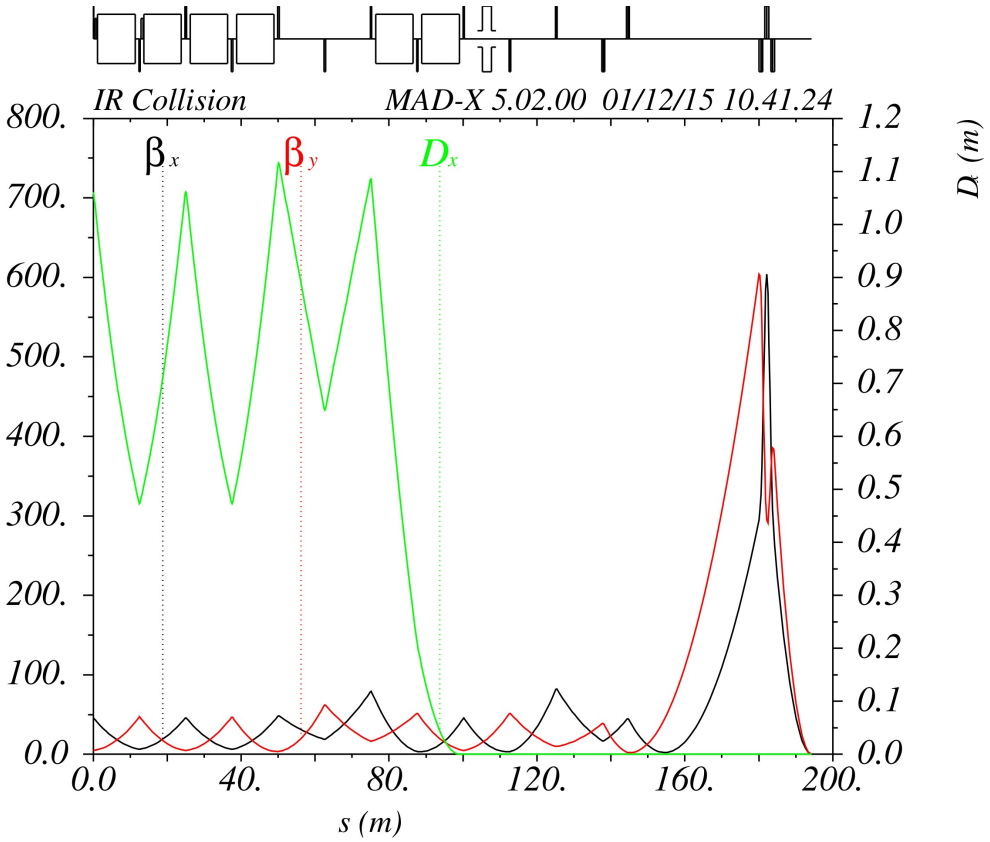

Figure 9: The optics for the colliding section in colliding mode for the high energy configuration.

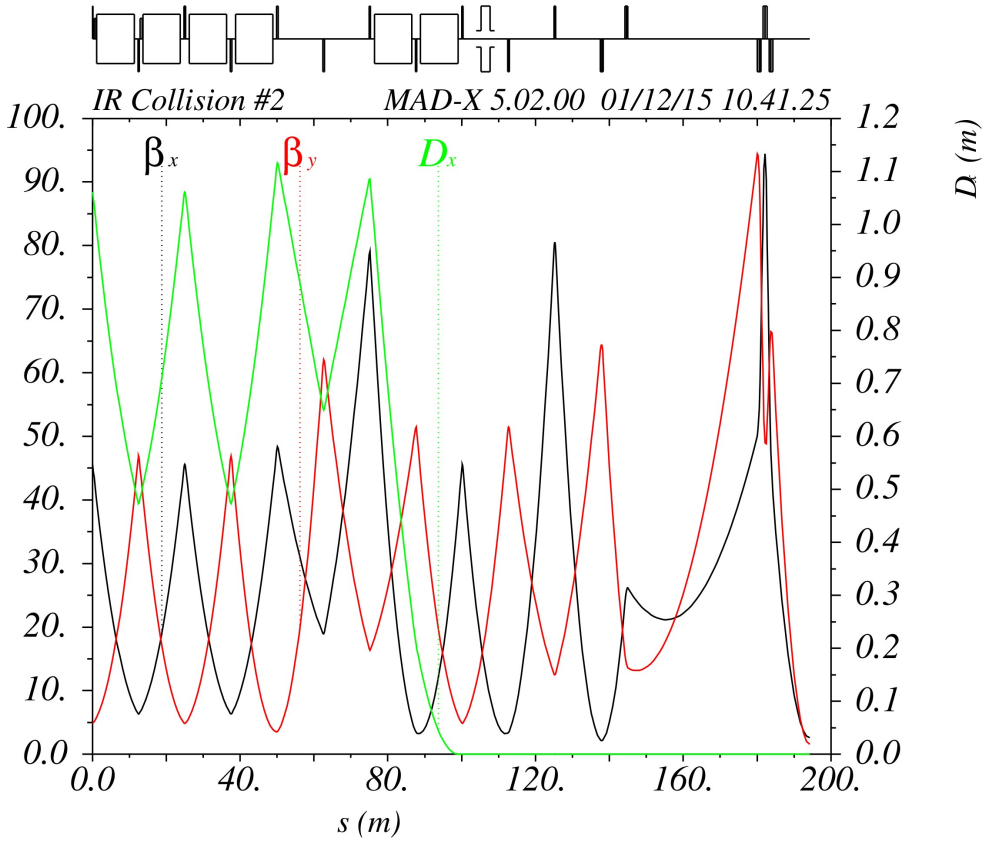

Figure 10: The optics for the colliding sector in the non-colliding mode.

Non-Colliding Section (Dispersion Free)

Three straight sections are non-colliding sections without dispersion. The β_{max} are kept small in this section. Additional families of sextupoles can be added to correct for amplitude dependent tunes. Empty drift spaces are available for other equipment that can be added as well. Fig. 11 shows this section from the high energy configuration.

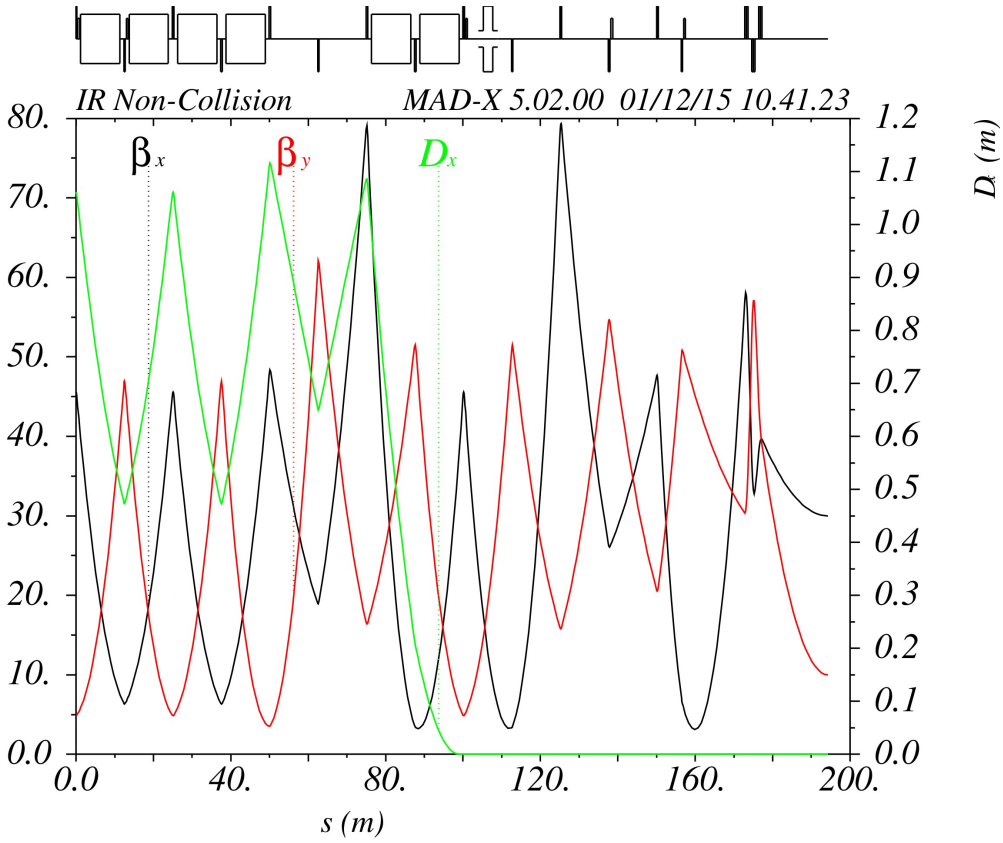

Figure 11: The dispersion free non-colliding section. There are three of these in the ring.

Non-Colliding Section (with Dispersion)

There is one straight section that includes dispersion. The main purpose of this section is to include the Robinson Wiggler [2], denoted as RW, to control the emittance in the low energy configuration. The goal emittance at low energy is 106 nm (5 GeV), compared to high energy 53 nm (20 GeV). Taking into account that the emittance changes as the square of the energy, the low energy emittance reduces by factor of 16. Furthermore, the emittance requirement increases by a factor of 2. Thus, the low energy configuration needs to be increased by a factor 32 over the high energy configuration. To achieve this, we reduce the horizontal phase advance of the cell to about 60°[2] from the high energy configuration giving us about a factor 3 increase in emittance. To get an additional factor of 10 required, a RW is employed. The RW consists of 4 dipoles with gradients, see Fig. 12. The RW changes the damping partition number, denoted as $\mathcal{D}$, as:

2 Choosing a phase advance lower than 60° would require negative bends for the dispersion suppressor.

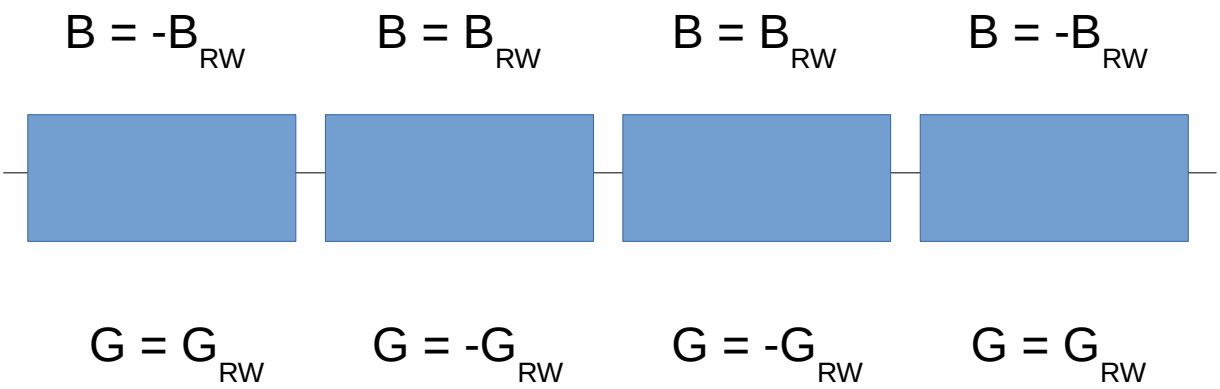

Figure 12: A schematic of a Robinson Wiggler. For the RW used in the ring, L_{RW}=7.0 m, ρ_{RW}=170.0 m, B_{RW}=0.09807 T and $G_{RW}=dB_{RW}/dx$=0.3919 T/m.

$$\Delta \mathcal{D} = \langle \eta \rangle \frac{1}{B_{RW}} \frac{dB_{RW}}{dx} \frac{4 L_{RW} \rho}{2 \pi \rho_{RW}^2} \left(1 + \frac{4 L_{RW} \rho}{2 \pi \rho_{RW}^2} \right)$$

where $<\eta>$ is the averaged dispersion through the RW, B_{RW}, L_{RW}, ρ_{RW} and dB_{RW}/dx are the dipole field, length, bending radius and gradient of a RW magnet, ρ is the bending radius of the ARC dipole magnets. Note, for positive dispersion – the damping partition number is increased – which decreases the emittance, however, when the dispersion is negative, the emittance is increased. Figs. 13-15 show the optics of the low, middle and high energy configuration through half the RW respectively.

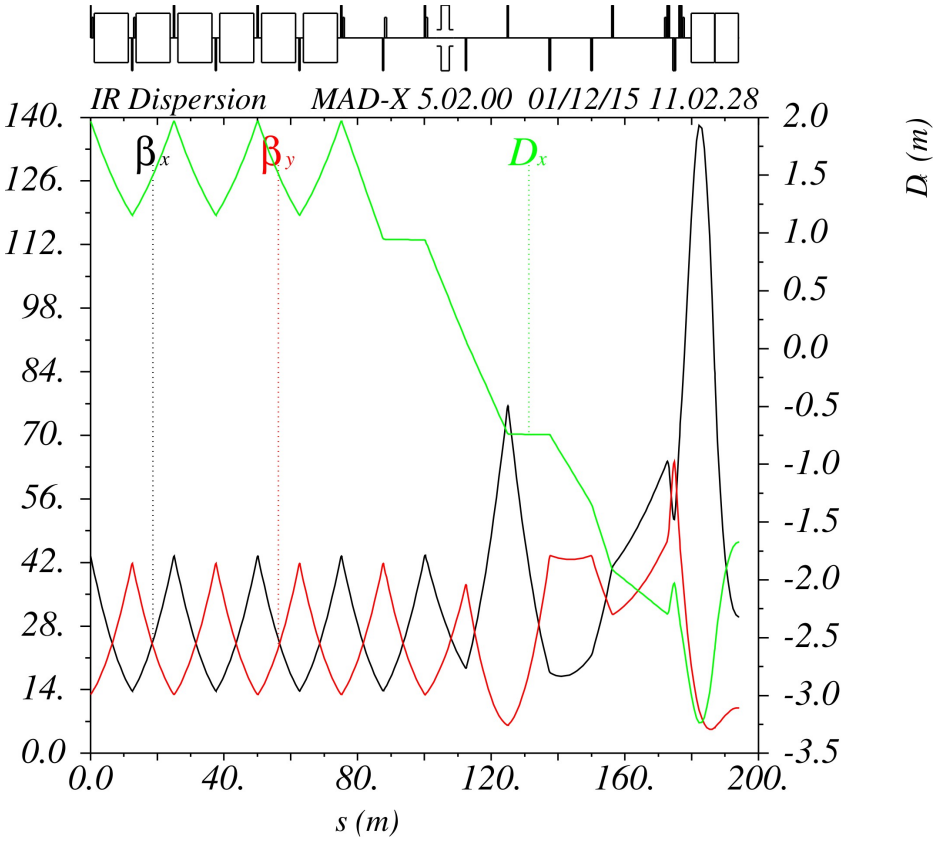

Figure 13: The straight section with 1/2 of the RW. The optics for the low energy configuration with the RW on. The RW is included when matching to the ARCS. Note the large β-functon through the RW.

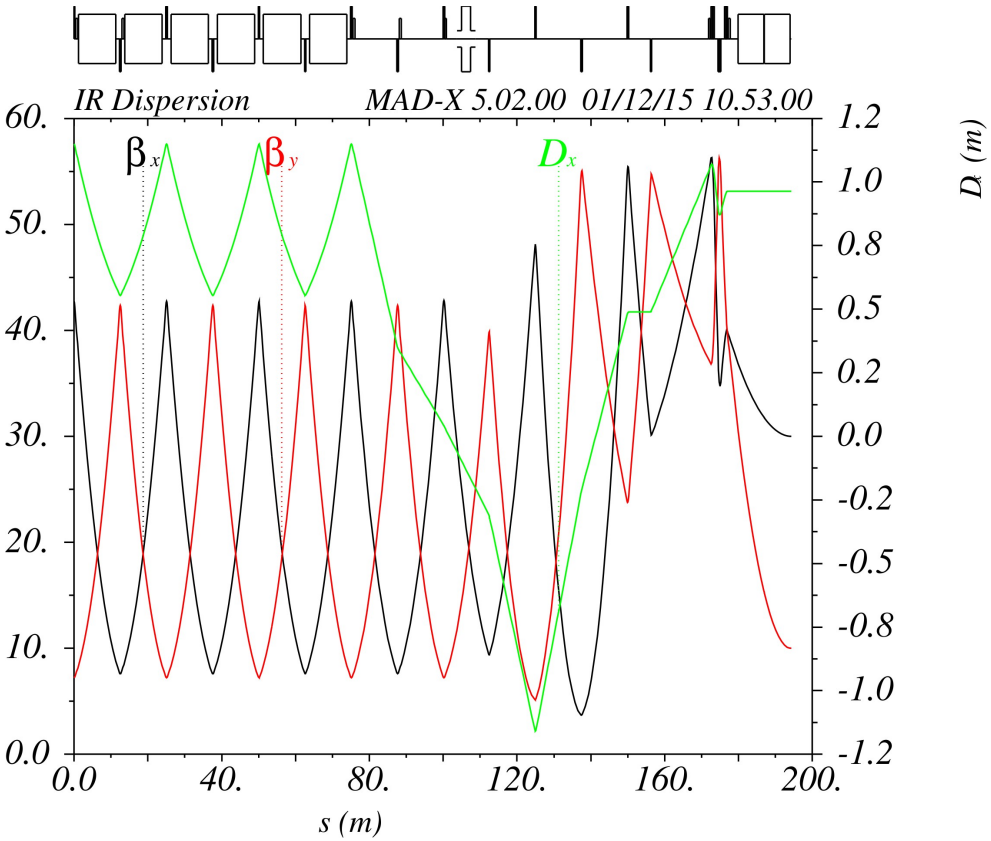

Figure 14: The middle energy configuration. The RW is off.

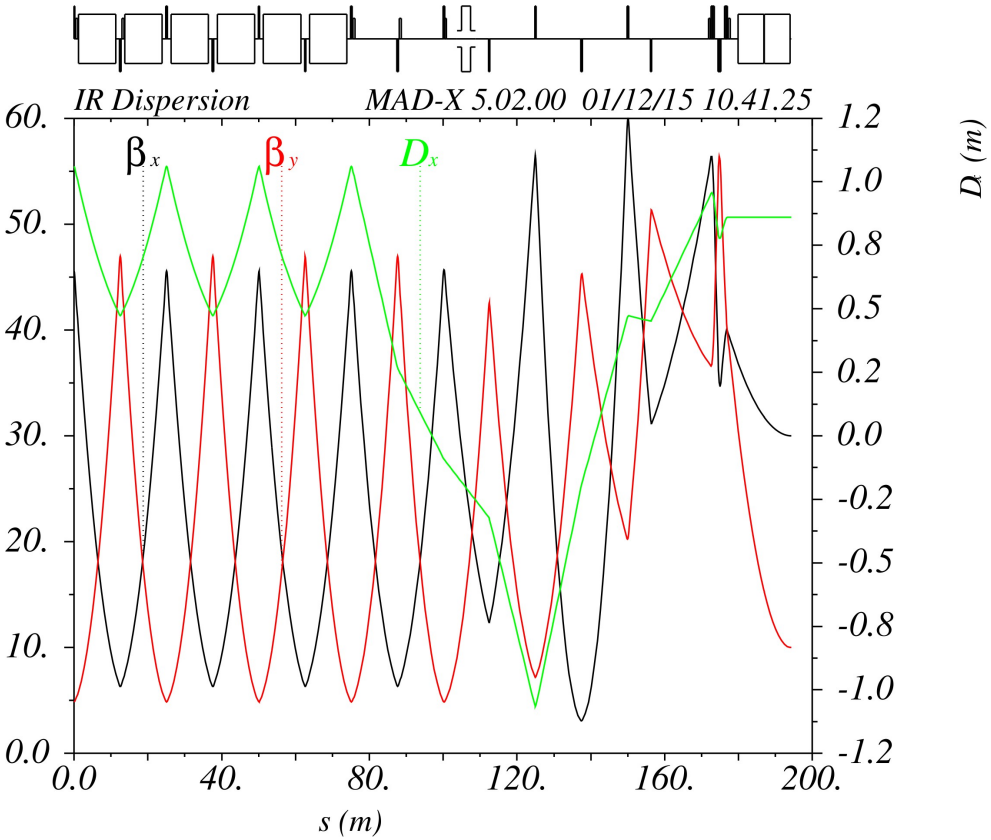

Figure 15: The high energy configuration. The RW is off.

The Ring

The ring consists of 6 ARCs and 6 straight sections described previously. Note, there is freedom to shuffle these straight sections to different IPs. Table 5 shows the ring properties using MADX [6]. The optics for the ring are shown in Figs. 16-18 for the three energy configurations.

The emittance which depends on the radiation integrals varies with the momentum spread. The damping partition number changes with momentum as [2]:

$$\frac{\Delta \mathcal{D}}{\delta} = \frac{2\int K^2 \eta^2 ds}{\oint ds/\rho^2}$$

where K is the quadrupole strength, η is the dispersion, ρ is the bending radius of the dipole magnets, s is the position along the beam trajectory and δ is the momentum spread. Note, $\Delta\mathcal{D}/\delta$ increases as the horizontal phase advance of the cell decreases. Thus, the change of emittance with momentum spread becomes larger in the low energy configuration.

Figs. 19-21 shows the momentum dependence of the emittance for the three energy configuration. The low energy configuration has a pole due to the shift in damping parameter from the RW. Whether this causes a problems for the luminosity needs to be determined.

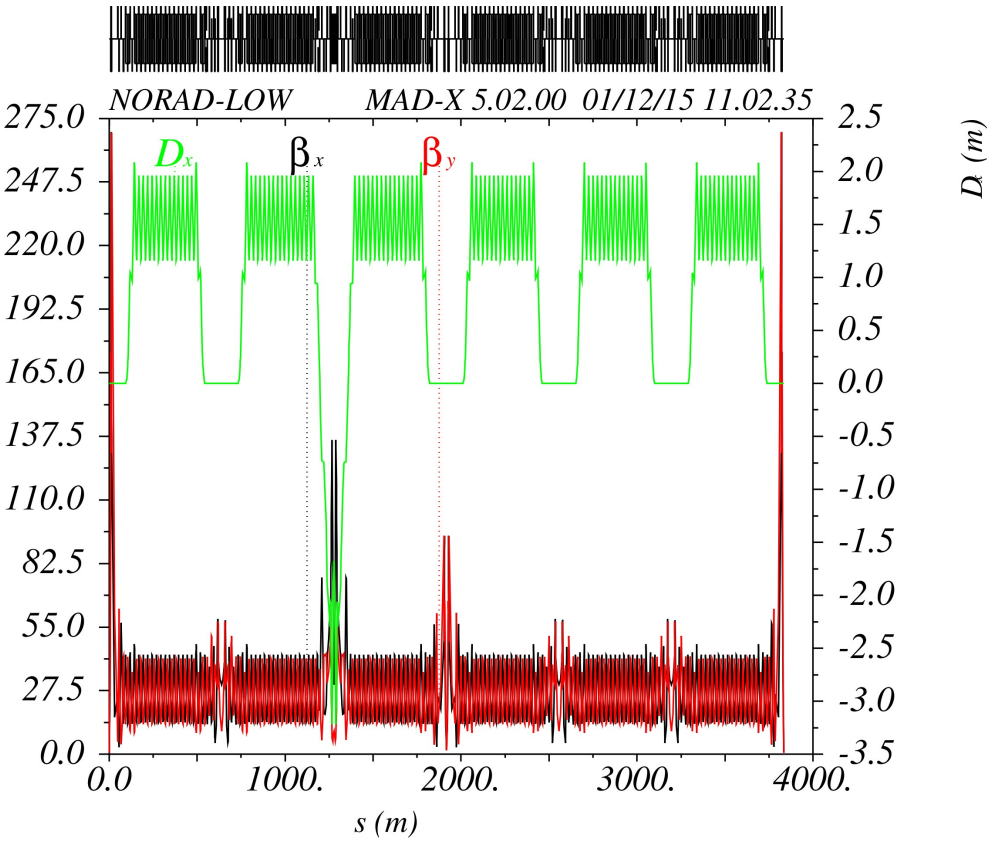

Figure 16: The ring in the low energy configuration.

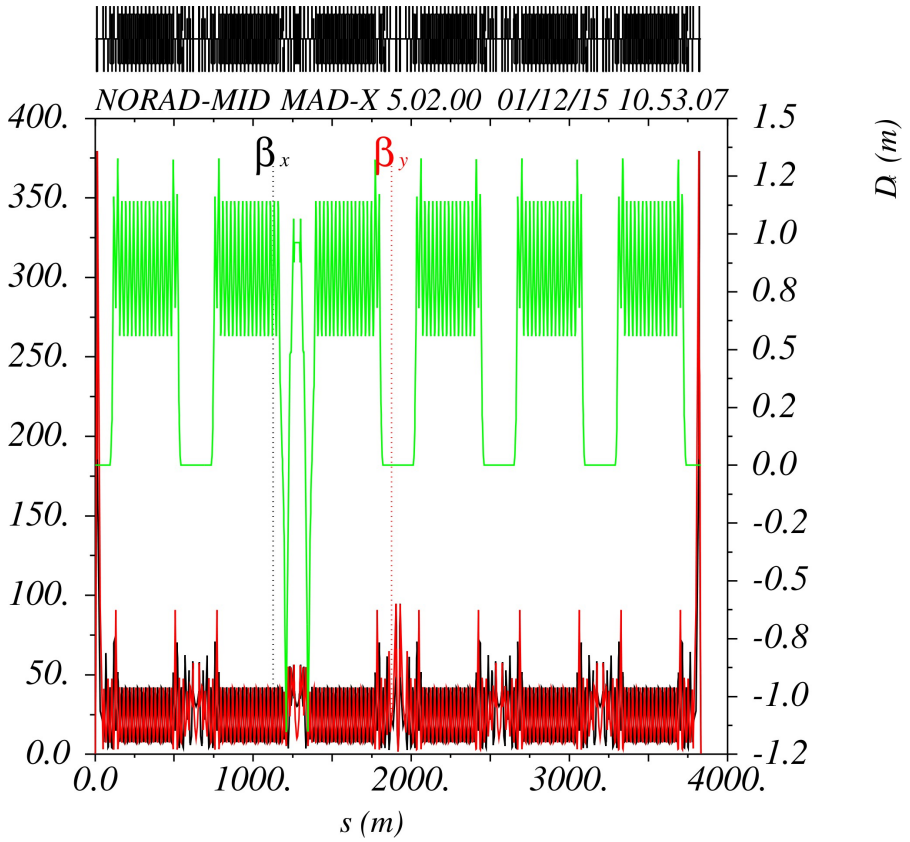

Figure 17: The ring in the middle energy configuration.

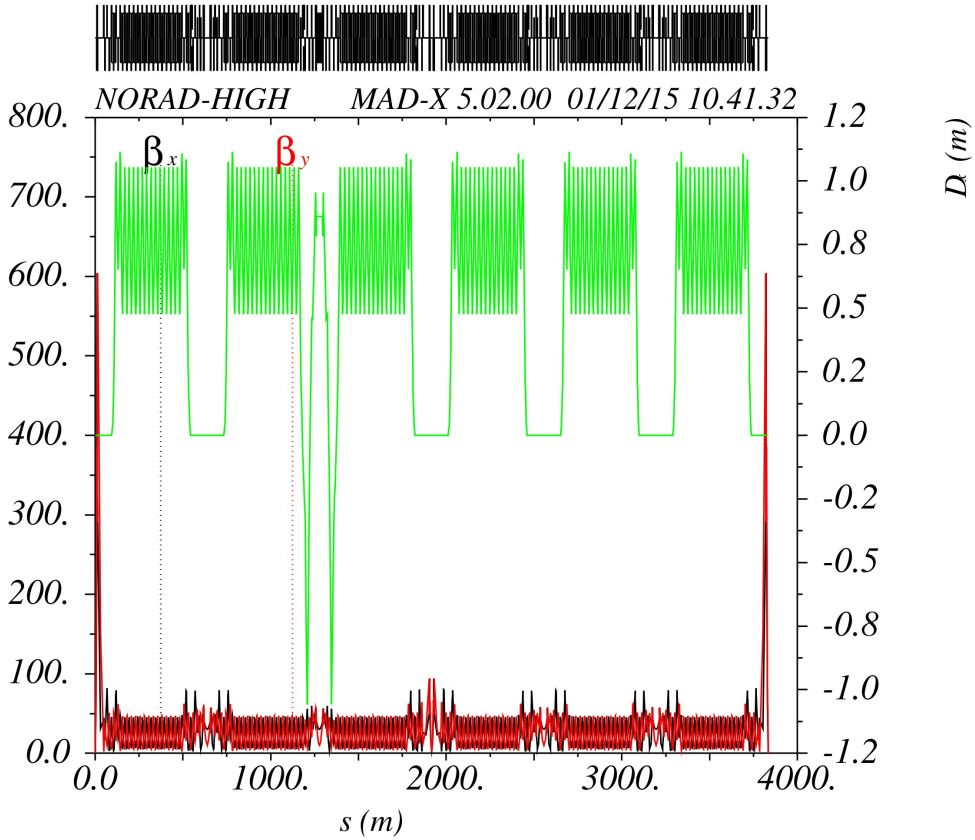

Figure 18: The ring in the high energy configuration.

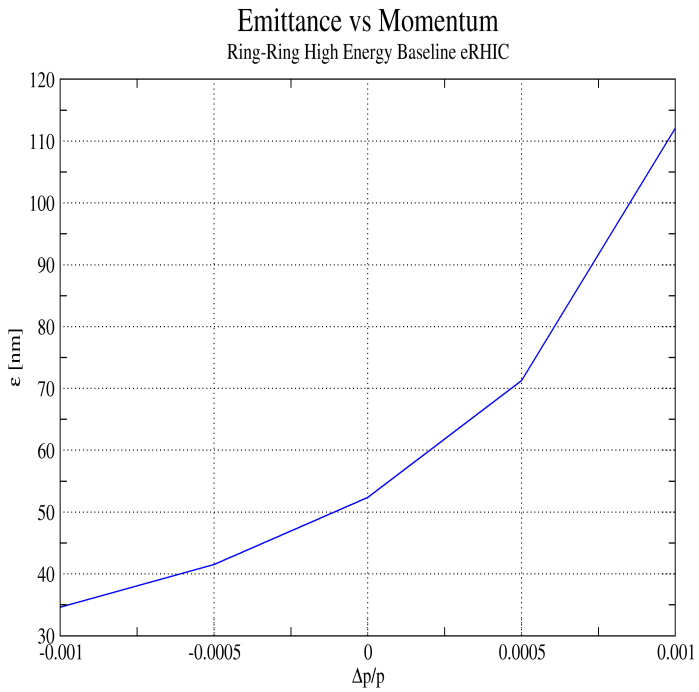

Figure 19: Emittance versus momentum spread for the high energy configuration. $\Delta D/\delta \approx 520$

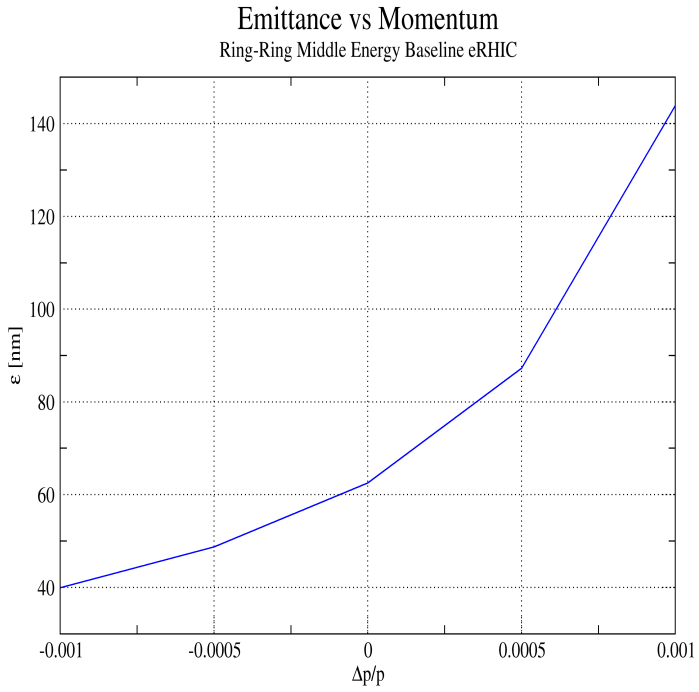

Figure 20: Emittance versus momentum spread for the middle energy configuration. $\Delta D/\delta \approx 560$

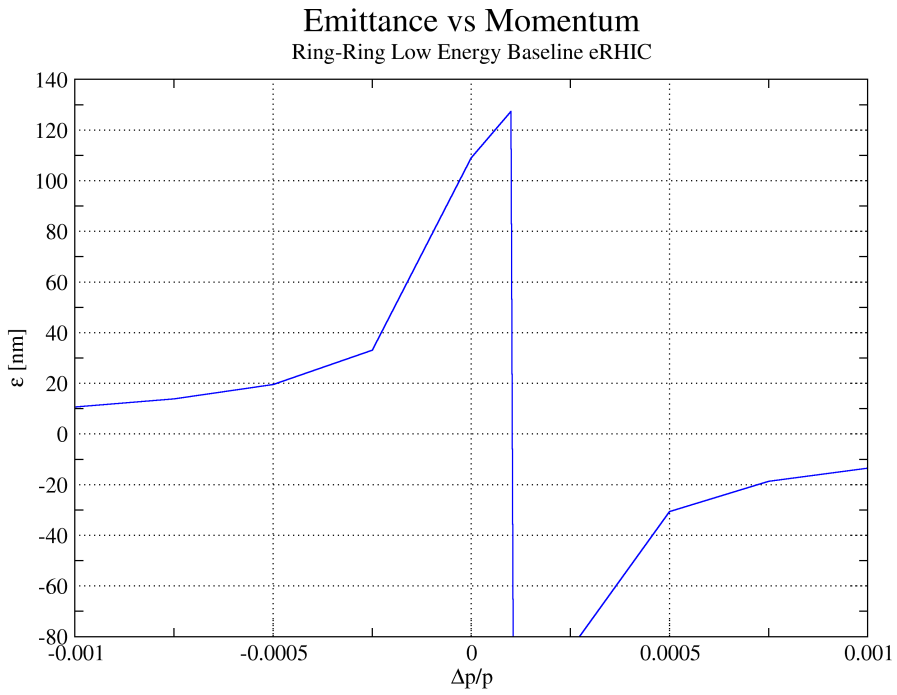

Figure 21: Emittance versus momentum spread for the low energy configuration. $\Delta\mathcal{D}/\delta \approx 911$. Note, the pole for 0.0001 = Δp/p. This is due in part to using the Robinson Wiggler to shift the damping partition number to, $\mathcal{D}=0.9003$.

Conclusion

A design for the electron storage ring to be used in the Ring-Ring eRHIC project is proposed. This ring must fit in the existing RHIC tunnel and have its IP points match the existing IP points of RHIC. This initial design has enough space to be able to use the existing PEP II quadrupoles [4]. Further work needed to be done:

1. Check the rings geometry to the existing RHIC for any conflicts.
2. Redesign with the PEP II quadrupoles.
3. Extend the two families of sextupoles for correction of higher chromatic and amplitude dependent tune effects.
4. Design for real RF cavities, instead of the six RF cavities used.
5. Add additional devices such as BPMs, orbit correctors, spin rotators, wigglers, etc.
6. Beam tracking studies for dynamic aperture, polarization preservation, momentum dependence and beam-beam luminosity.
7. Can we use this ARC design for future upgrade(s)?

Configuration	Low	Middle	High
Energy [GeV]	5	20	20
Design Tunes	28.72, 29.82	38.28, 39.18	40.28, 41.18
Cell Phase Adv [°]	61.76, 65.23	88.06, 91.37	95.07, 111.82
Cell Length [m]	25.047651		
Dipole Length [m]	10.123825		
ρ [m]	309.361304		
Circumference [m]	3833.845181		
Momentum Compaction	0.00231	0.00123	0.00110
Natural Chrom	-45.375, -43.148	-66.414, -67.209	-80.293, -76.710
Horizontal Chrom	1.83, 140.4, 46738	1.86, 359.5, 83866	1.85, 725.9, 673201
Vertical Chrom	1.88, 129.9, 26794	1.90, 186.6, 11078	1.88, -2030.2, 884622
α_{xx}, α_{xy} or α_{yx}, α_{yy}	-272.3, -850.5, -165.3	37.35, -2315, 32.52	4661, 3748, 3348
β_{max} [m]	269.1	379.4	603.8
Horizontal ε [nm]	109.3	62.52	52.37
J_x	0.0994339	0.99509099	0.99512338
J_E	2.90063429	2.00490632	2.00487382
U_0 [MeV/turn]	0.187	45.755	45.754
Beam Current [Amp]	0.925	0.508	0.508
Total SR power [MW]	0.173	23.243	23.243

Table 5: Parameters for the ring in the three energy configurations of the baseline design. The "Design Tunes", "Cell Phase Adv" and "Natural Chrom" rows give the "horizontal, vertical" values. The "Horizontal Chrom" and "Vertical Chrom" rows show the "1st order, 2nd order, 3rd order" chromaticity values from PTC in MADX with two families of sextupoles in the cells. The column "α_{xx}, α_{xy} or α_{yx}, α_{yy}" gives the amplitude dependent tune effects due to the sextupoles. The high energy configuration has very strong chromatic effects which can be reduced by setting the vertical tune to 39.18 (below the horizontal tune).

Acknowledgments

We'd like to thank Scott Berg, Vadim Ptitsyn and Dejan Trbojevic for many useful discussions.

Bibliography

[1] E.C. Aschenauer, S. Berg, M. Blaskiewicz, M. Brennan, A. Fedotov, W. Fischer, V. Litvinenko,C. Montag (chair), R. Palmer, B. Parker, S. Peggs, V. Ptitsyn, V. Ranjbar, S. Tepikian, D. Trbojevic, F. Willeke, *Report of the eRHIC Ring-Ring Working Group*, eRHIC/46 (2015).
[2] S. Y. Lee, *Accelerator Physics*, World Scientific (1999).
[3] R. Ropert, *Low Emittance Lattices*, CERN 95-06, 147-166 (1995).
[4] *PEP-II Conceptual Design Report*, SLAC-418 (1993)
[5] Mario Conte, William W. MacKay, *An Introduction to the Physics of Particle Accelerators*, World Scientific (2008).
[6] *The MADX Program*, http://mad.home.cern.ch/mad, MAD-X 5.02.00 (2014)